AGU PUBLICATIONS

Geophysical Research Letters

RESEARCH LETTER
10.1002/2015GL067262

**Key Points:**
- Cold pools are affected by surface heat fluxes
- Convection over the ocean and land is differentially affected by surface heat fluxes on cold pools
- Flux boundary conditions for convection generally give unrealistic convection organization

**Supporting Information:**
- Figures S1–S4 and Tables S1–S4

**Correspondence to:**
P. Gentine,
pg2328@columbia.edu

**Citation:**
Gentine, P., A. Garelli, S.-B. Park, J. Nie, G. Torri, and Z. Kuang (2016), Role of surface heat fluxes underneath cold pools, *Geophys. Res. Lett.*, *43*, 874–883, doi:10.1002/2015GL067262.

Received 7 DEC 2015
Accepted 30 DEC 2015
Accepted article online 5 JAN 2016
Published online 22 JAN 2016



# Role of surface heat fluxes underneath cold pools

**Pierre Gentine[1], Alix Garelli[1], Seung-Bu Park[1], Ji Nie[2], Giuseppe Torri[3], and Zhiming Kuang[4]**

[1]Earth and Environmental Engineering, Earth Institute, School of Engineering and Applied Science, Columbia University, New York, New York, USA, [2]Earth and Environmental Sciences, Lamont Doherty Laboratory, Columbia University, New York, New York, USA, [3]Earth and Planetary Sciences, Harvard University, Cambridge, Massachusetts, USA, [4]Earth and Planetary Sciences and School of Engineering and Applied Sciences, Harvard University, Cambridge, Massachusetts, USA

**Abstract** The role of surface heat fluxes underneath cold pools is investigated using cloud-resolving simulations with either interactive or horizontally homogenous surface heat fluxes over an ocean and a simplified land surface. Over the ocean, there are limited changes in the distribution of the cold pool temperature, humidity, and gust front velocity, yet interactive heat fluxes induce more cold pools, which are smaller, and convection is then less organized. Correspondingly, the updraft mass flux and lateral entrainment are modified. Over the land surface, the heat fluxes underneath cold pools drastically impact the cold pool characteristics with more numerous and smaller pools, which are warmer and more humid and accompanied by smaller gust front velocities. The interactive fluxes also modify the updraft mass flux and reduce convective organization. These results emphasize the importance of interactive surface fluxes instead of prescribed flux boundary conditions, as well as the formulation of surface heat fluxes, when studying convection.

## 1. Introduction

Rain falling from convective clouds evaporates and generates a cold unsaturated downdraft [*Betts and Silva Dias*, 1979]. As this air encounters the surface, it spreads out horizontally as a density current [*Lafore and Moncrieff*, 1989; *Xu and Moncrieff*, 1994; *Grandpeix and Lafore*, 2010], named cold pool, the gust front of which can lift air and generate updrafts. The efficiency of this lifting mechanism depends on the characteristics of the cold pools, and the resulting updrafts can help trigger [*Moncrieff and Liu*, 1999; *Khairoutdinov and Randall*, 2006; *Böing et al.*, 2012; *D'Andrea et al.*, 2014], maintain, and organize convection [*Liu and Moncrieff*, 2004; *Böing et al.*, 2012; *Jeevanjee and Romps*, 2013; *Feng et al.*, 2015; *Muller and Bony*, 2015]. Cold pools trigger convective updrafts through either mechanical forcing at their gust front or through thermodynamic forcing at their edge, which is typically moister than the rest of the cold pool [*Schlemmer and Hohenegger*, 2015], or through a combination of both [*Li et al.*, 2014; *Jeevanjee and Romps*, 2015; *Torri et al.*, 2015]. As such, cold pools are an essential component of our understanding of convection and convective aggregation.

As cold pools spread, the cold air overlays a warmer surface and this generates substantial turbulent instability near the surface, which intensifies the surface sensible and latent heat fluxes [*Ross et al.*, 2004]. The resulting stronger heat fluxes underneath cold pools can erode the density anomaly of the cold pools and potentially facilitate their death [*Qian et al.*, 1998; *Ross et al.*, 2004]. On the other hand, the reduced cold pool density anomaly diminishes the gust front velocity and spreading [*Simpson*, 1969]. This, in turn, limits turbulent mixing of cold pool air with the environment [*Simpson*, 1969], which reduces the cold pool warming and moistening by mixing, and slows down the cold pool death. Thus, the reduced mixing competes with the surface heat fluxes for the cold pool life cycle.

If surface fluxes modify cold pool characteristics, such as their number, area, temperature, and humidity anomalies, this could potentially alter the generation of new convective cells and could also impact the updraft entrainment, since the organization of the subcloud layer by cold pools results in wider updrafts that entrain less [*Betts*, 1984; *Khairoutdinov and Randall*, 2006; *Schlemmer and Hohenegger*, 2014]. To our knowledge, there are only limited studies discussing the surface heat flux heterogeneities underneath cold pools [*Qian et al.*, 1998; *Ross et al.*, 2004]. The aim of the present study is thus to answer the following two questions: (1) What is the role of surface heat fluxes on the characteristics of cold pools over an oceanic and continental surface? (2) How do changes in cold pool characteristics influence convective updrafts, entrainment, and the organization of convection? To investigate these questions, we perform cloud-resolving simulations of cold pools over oceanic and land surfaces with and without interactive surface heat fluxes.

## 2. Method

### 2.1. Model

We use the System for Atmospheric Modeling, version 6.10.8 in cloud-resolving model mode [*Khairoutdinov and Randall*, 2003], which solves the anelastic equations of motion. Doubly periodic boundary conditions are applied in the horizontal. A sponge layer is used in the upper third part of the domain to damp gravity wave reflection. A 1.5 order closure prognostic turbulent kinetic energy scheme is used for subgrid-scale parameterization. We use the Morrison scheme with binned microphysics [*Morrison and Gettelman*, 2008]. A 500 m grid size is used in the horizontal. The vertical grid size increases from 20 m at the lowest level to 704.5 m at the highest, with 20 grid points below 1 km to better resolve the boundary layer. The computational domain consists of $256 \times 256 \times 64$ grid points and covers $128 \times 128 \times 17.8075$ km$^3$. The time step is 10 s so as to ensure that the Courant-Friedrisch-Lewy condition ($<0.7$) is satisfied during the entire simulation.

Here we focus on cases of convection without important shear and we purposely do not consider mesoscale convective systems and squall lines since they are very much influenced by the position and intensity of shear [*Weisman and Rotunno*, 2004], which strongly complicates the life cycle and propagation of cold pools. The initial sounding, large-scale conditions, and radiation are taken from the GARP Atlantic Tropical Experiment averaged over the period 30 August to 18 September 1974 [*Betts*, 1974] without vertical wind shear (Tables S1 and S2 in the supporting information). Radiation is prescribed and held constant throughout the 48 h simulation. The main characteristics of the simulations are summarized in Table S3. We remove the diurnal cycle since our interest is not in the radiation-induced changes of surface temperature. In the absence of very large convective systems, the radiation effect of individual clouds on surface temperature is relatively minor [*Lohou and Patton*, 2014]. Finally, we compute the updraft mass flux on parcels with condensation (larger than 0.01 g kg$^{-1}$) and with vertical velocity above 0.1 m s$^{-1}$.

To assess the role of surface heat fluxes on cold pools, four types of simulations are performed: an oceanic (OCEAN) and a land scenario (LAND), each with either interactive surface fluxes (INT)—computed using Monin-Obukhov stability functions [*Businger et al*., 1971]—or fixed surface fluxes (FIX), homogenous in the horizontal. The FIX runs use the time- and domain-average surface fluxes from the corresponding INT run (either OCEAN or LAND), so as to ensure that the FIX and INT simulations have the same mean surface heat fluxes.

The roughness length is set to 0.001 m for the OCEAN scenario and 0.035 m for the LAND. For the INT case, sea surface temperature is prescribed to 300 K over the ocean. The land surface is represented as a saturated surface (swamp) using an ocean mixed layer model with an inertia equivalent to 0.05 m of water [*Cronin and Emanuel*, 2013]. The surface temperature over land is relaxed to 300 K with a 30 min time scale to allow for realistic buildup of cold pool-induced surface heterogeneities and also to avoid substantial temporal changes in the domain-average surface temperature. For the FIX cases, the surface sensible and latent heat fluxes in the OCEAN runs are set to 8.79 and 55.6 W m$^{-2}$, respectively, and to 13 and 164.8 W m$^{-2}$ for the LAND runs. A summary of the statistics of sensible and latent heat fluxes below cold pools in the INT cases is presented in Table S4 (supporting information).

To obtain reliable statistics, 16 ensemble members are generated for each simulation by perturbing the initial conditions using different seeds for the random number generator. We tested the resolution sensitivity of our results by changing the horizontal grid spacing to 250 m and 1 km and doubling the vertical resolution, and we did not find any significant changes in our conclusions. Cold pools and updrafts statistics are computed every 6 h on the model output snapshots across the 16 ensemble members. Since most cold pools die in less than 6 h (see Figure S1), this choice of sampling frequency seems adequate.

### 2.2. Cold Pool Identification and Characteristics

Cold pools are identified using virtual temperature $T_v$—a quantity directly related to air density—at the first model level [*Torri et al*., 2015] (Figure 1a). Cold pool regions are determined using a $k$ mean unsupervised image segmentation based on two clusters, cold pools and environment (Figure 1b). Each cold pool region is given a unique identification number (ID) (o), so that its individual characteristics can be analyzed. The algorithm performs a breadth-first search [*Skiena*, 2008] to determine all the pixels that are 4-connected to an initial pixel within the cold pool cluster. When the search is terminated, the algorithm recognizes the subset of connected pixels as a single cold pool and assigns an ID number to each subset. Cold pools with radii smaller than 3 km are considered too small and are discarded from the analysis. Finally, we compute the area,

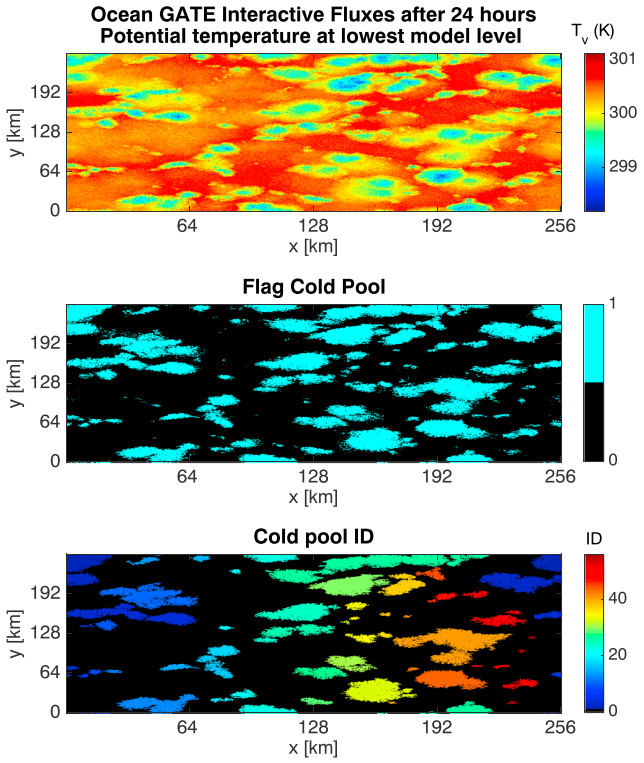


**Figure 1.** Snapshot of (top) surface virtual temperature after 24 h of simulation in the OCEAN case with interactive INT fluxes; *k* clustering image classification based on two clusters corresponding to the (middle) environment (0 flag) and cold pools (1 flag); and (bottom) cold pool ID number based on the above classification. Only cold pools larger than $3 \times 3$ km$^2$ are kept in the cold pool ID analysis.

perimeter, and the horizontal-mean temperature and humidity anomalies of each cold pool. The mean gust front velocity, $\bar{c}_*$, along each cold pool perimeter $l$ is computed using Gauss' theorem, assuming no fluid flow across the boundary (a reasonable assumption in the horizontal):

$$\bar{c}_* l = \oint_l c_* \mathrm{d}l = \iint_S \nabla \cdot \mathrm{u}_H \mathrm{d}S, \qquad (1)$$

with $\mathrm{u}_H$ the horizontal wind and $S$ the cold pool area. The divergence is computed using a finite difference approximation.

### 2.3. Entrainment Analysis

To understand the impact of changes in cold pools on the updraft characteristics, we use the isentropic analysis of *Kuang and Bretherton* [2006], which highlights the entrainment-dependent mass flux changes. This method uses a near-conserved thermodynamic variable, the frozen moist static energy (hereafter, MSE), $h = C_p T + gz + L_v q_v - L_f q_1$, with $C_p$ the dry air specific heat, $T$ the air temperature, $g$ the gravitational acceleration, $L_v$ and $L_f$ the latent heat of vaporization and freezing, and $q_v$ and $q_i$ the specific humidities of water vapor and ice. MSE is conserved under vapor-liquid phase transitions and during the production and evaporation of ice and the removal (or addition) of liquid precipitation. It is not conserved under the removal of ice, but the overall impact is small [*Kuang and Bretherton*, 2006].

The vertical gradient of a conserved updraft scalar $\psi_u$, assuming a steady state plume entraining environmental air scalar with value $\psi_{\mathrm{env}}$ at a constant rate $\epsilon$ and with a source per unit height $S_\psi$, is

$$\frac{\partial \psi_u}{\partial z} = \epsilon(\psi_{\mathrm{env}} - \psi_u) + S_\psi. \qquad (2)$$

Assuming that $S_\psi = 0$ and that the updraft coverage is small—so that $\psi_{\mathrm{env}} \approx \overline{\psi}$, the horizontal mean—this equation can be integrated from cloud base (defined as the height of lowest cloud fraction maximum) to a height $z$, assuming that the entrainment rate is constant in height, to yield

$$\psi_u(z) = \left(\psi_u(\mathrm{LCL}) e^{\epsilon \mathrm{LCL}} + \int_{\mathrm{LCL}}^{z} \epsilon \overline{\psi}(z') e^{\epsilon z'} \mathrm{d}z'\right) e^{-\epsilon z}, \qquad (3)$$

where LCL is the cloud base altitude and $\psi_u$(Lifting Condensation Level) is taken as the mean $\psi_u$ across all updrafts at the LCL, as variations in $\psi_u$ are only minor at the LCL [*Kuang and Bretherton*, 2006]. Therefore, each entrainment rate $\epsilon$ defines an updraft MSE profile. We bin the entrainment rates according to $10^{-x}$ (in m$^{-1}$), with $x$ ranging from 2.3 to 6 with 0.025 increments, and compute the corresponding vertical profiles of $\psi_u(z)$ (Figure 2 (top), dashed yellow lines).

## 3. Results

### 3.1. Changes in Cold Pool Characteristics

In the OCEAN INT case, most cold pools are smaller than 500 km$^2$ (Figure 3a). The surface virtual temperature $T_v$ anomaly is nearly normally distributed (Figure 3c), with mean −0.8 K, standard deviation 0.19 K, 0.0044

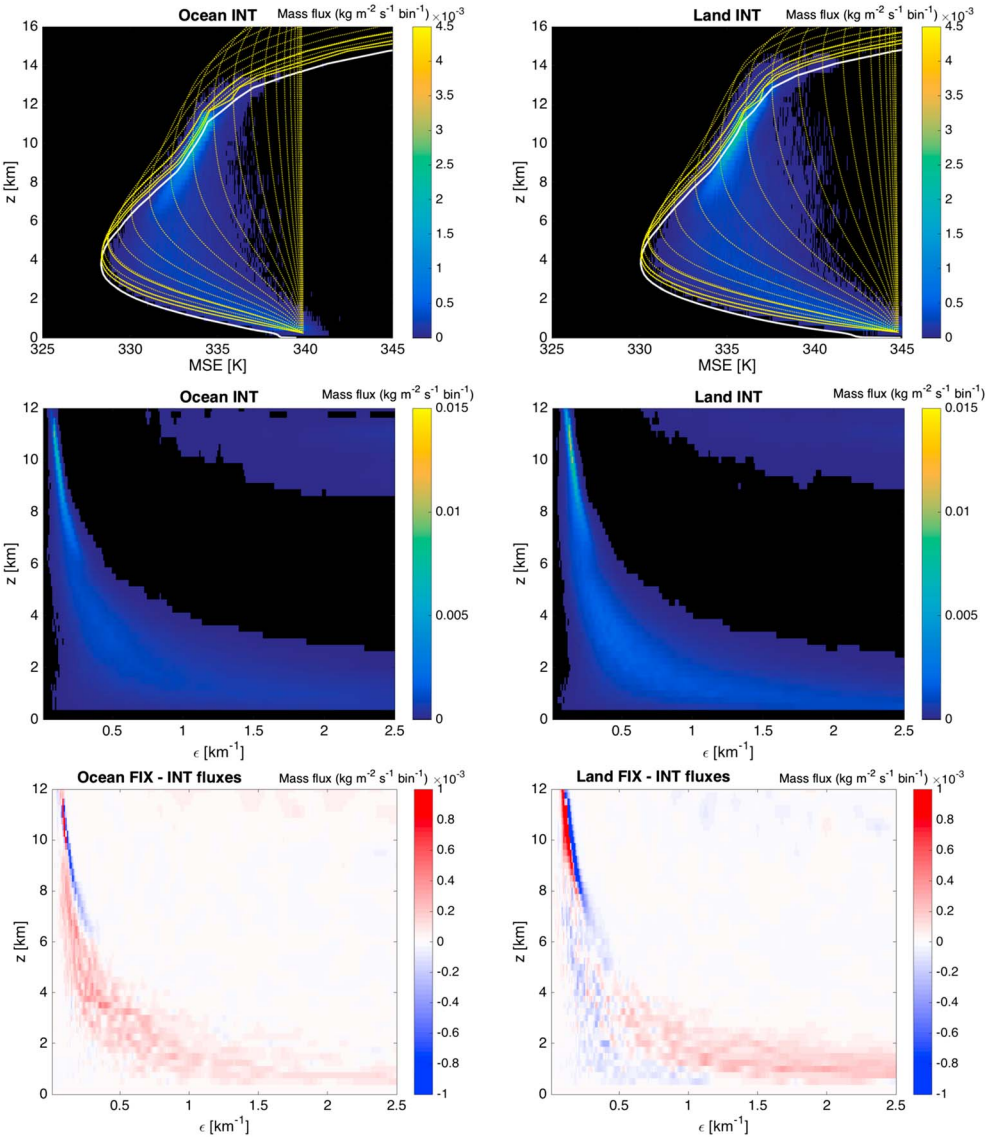


**Figure 2.** Time averaged: (top) mass flux binned based on MSE and height for the interactive INT case for the (left column) OCEAN and (right column) LAND cases. Black areas denote mass flux bin less than $10^{-4}$ kg m$^{-2}$ s$^{-1}$ bin$^{-1}$. Data were binned based on 0.1 K MSE increments along the *x* axis and according to the model resolution in the vertical. Yellow dashed lines representing binning of fractional entrainment rates with sampling based on $10^{-\text{bin}}$, with bin ranging from 2.5 to 5 with 0.1 increments. Note that the mass flux is small right above the LCL in the OCEAN case. The white line represents the mean horizontal MSE value. (middle) Mass flux binned as a function of the entrainment rate and height. A fractional entrainment binning of $10^{-\text{bin}}$, with bin ranging from 2.5 to 5 with 0.1 increments, was used. Black areas denote mass flux bins less than $10^{-4}$ kg m$^{-2}$ s$^{-1}$ bin$^{-1}$, and upper right mass flux areas have magnitude less than $10^{-5}$ kg m$^{-2}$ s$^{-1}$ bin$^{-1}$. (bottom) Difference in mass flux between the fixed and interactive cases binned as a function of height and entrainment rate (assumed to be constant in the bulk plume model). The same entrainment binning was used.

skewness (0 for a normal distribution), and 2.6 kurtosis (3 for a normal distribution). The gust front velocity is typically less than 1.5 m s$^{-1}$, with a mean of 0.55 m s$^{-1}$ and a standard deviation of 0.29 m s$^{-1}$ (Figure 3b). The specific humidity distribution is narrow and ranges from $-1$ to 0.3 g kg$^{-1}$, with most of the values clustered around $-0.4$ g kg$^{-1}$ (Figure 3d) and a mean and standard deviation of $-0.38$ g kg$^{-1}$ and 0.15 g kg$^{-1}$, respectively.

Over the OCEAN, cold pools in the INT case tend to be smaller (Figures 3a and 3e), as the increased heat flux heterogeneities reduce the density anomaly of the cold pools compared to the environment (Figure 3g) and, therefore, the strength of the gust front and horizontal spreading of the cold pools [*Emanuel*, 1994; *Grandpeix*

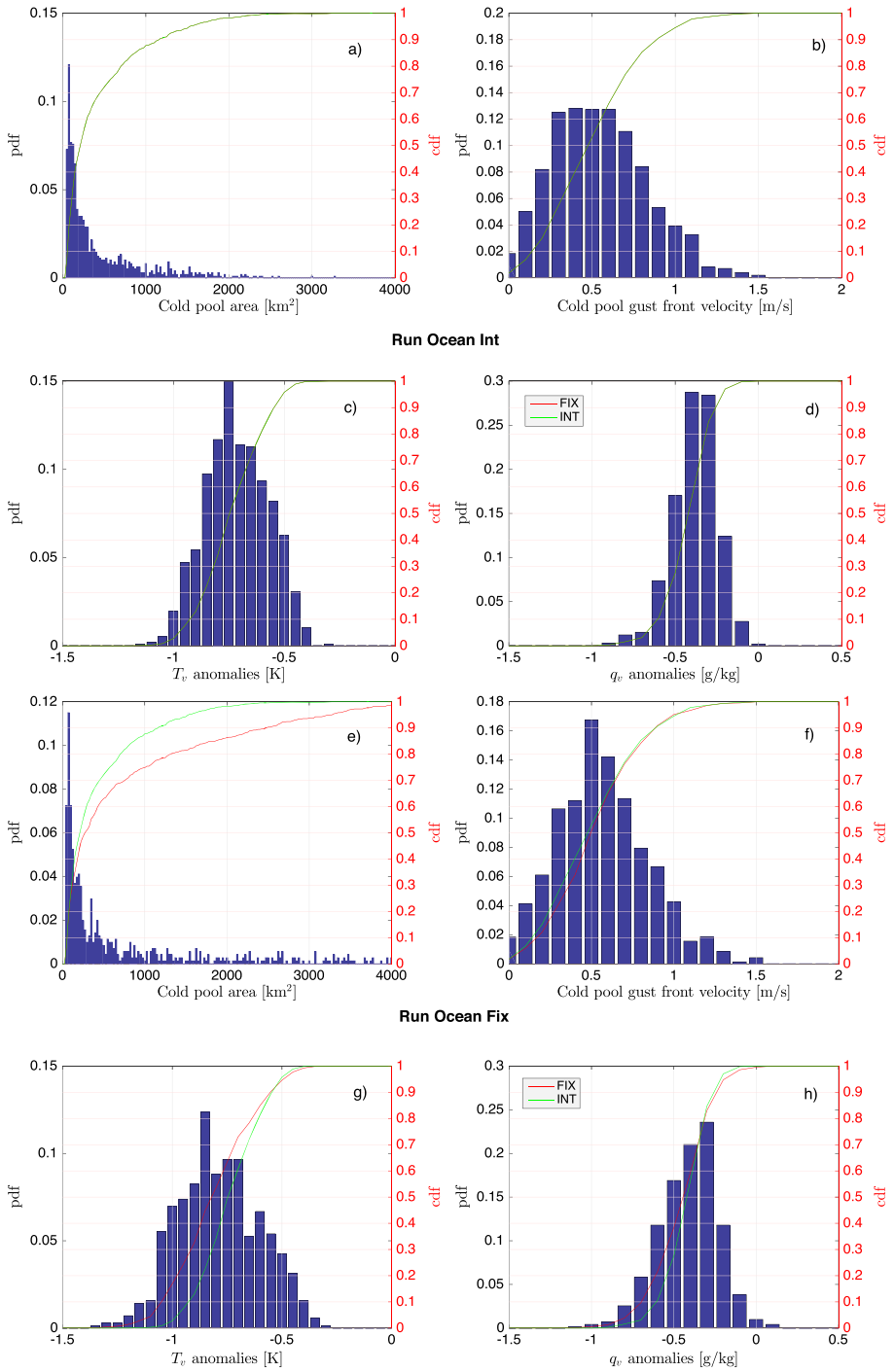


**Figure 3.** Cold pool statistics (area, gust front velocity, density temperature anomaly, and water vapor anomaly) pdf (bins) and cdf (continuous lines) for the OCEAN with (a–d) interactive INT fluxes and (e–h) fixed FIX fluxes based on the 16 simulations sampled every 6 h after an equilibrium is reached. Green line corresponds to the cdf of the interactive INT run, and red line corresponds to the fixed FIX runs.

*and Lafore*, 2010]. As a result, cold pools in INT are fairly confined yet more numerous (8 versus 5.6 cold pools on average at each time step), which reduces convective organization in INT. The overall probability distribution function (pdf) of the gust front velocities is very similar in the FIX and INT cases over the OCEAN (Figures 3b and 3f). We argue that this is because in the FIX case there are more large cold pools (Figure 3a). These large pools have smaller gust front velocity than smaller, younger, ones (not shown), since

the initial downdraft buoyancy is reduced during the horizontal spreading and entrainment of the cold pools. In fact, there are no systematic differences in the pdfs of the MSE (Figure S3) and area (Figure S4) of the downdrafts between the INT and FIX cases, which suggests that changes in the cold pool characteristics have to be the results of the fluxes underneath.

Over the OCEAN, as expected, cold pools are generally more humid in the INT case than in the FIX one (Figures 3d and 3h). Cold and dry air ventilation from the unsaturated downdrafts increases the specific humidity gradient at the surface, which, in the INT case, leads to substantial increase in latent heat fluxes underneath each cold pool. As a result, the specific humidity of the cold pools rises and the pdf of cold pool humidity shifts toward higher values, with a mean specific humidity anomaly of $-0.38\,\mathrm{g\,kg^{-1}}$ in INT and $-0.42\,\mathrm{g\,kg^{-1}}$ in FIX. The distribution also becomes narrower—with standard deviation of $0.15\,\mathrm{g\,kg^{-1}}$ in INT versus $0.2\,\mathrm{g\,kg^{-1}}$ in the FIX case (Figure 3h). Interestingly, the differences in the pdfs of temperature and humidity anomalies between the INT and FIX cases are nonetheless relatively small (Figures 3g and 3h), even though the number of cold pools and their size distributions are drastically affected (Figures 3a and 3e). This suggests that there is a compensation effect in the pdfs due to the presence of many large cold pools in the FIX case. Indeed, large cold pools have smaller (in absolute terms) temperature and humidity anomalies because of the spreading of the initial unsaturated downdraft anomaly over a wider distance and because of the continuous mixing with environmental air occurring at the cold pool edges [*Simpson*, 1969]. This mixing nearly compensates for the decreased heat fluxes below the cold pools in the FIX case. As a result, the pdfs are quite similar in FIX and INT. In other words, the spreading and mixing with environmental air in FIX increase the temperature and humidity by a comparable amount to that induced by surface flux heterogeneity underneath the (smaller) cold pools in INT.

In the LAND scenario, the virtual temperature anomalies are reduced in the INT case, with a mean of $-0.77$ K (Figure 4c), compared to $-0.95$ K in the FIX case (Figure 4g). Furthermore, in INT very few cold pools exhibit a surface $T_v$ anomaly lower than $-1.1$ K, whereas in FIX the anomaly can reach as low as $-1.5$K. This reduced buoyancy anomaly (in absolute value) is the result of the intense buoyancy flux underneath cold pools in the INT case (Table S4). In turn, the increased surface buoyancy flux reduces the strength of the density current [*Emanuel*, 1994; *Qian et al*., 1998; *Grandpeix and Lafore*, 2010], as evidenced by the change in the gust front velocity distribution (Figures 4b and 4f). The gust front is substantially faster in the FIX case (Figure 4f), with many values above $0.5\,\mathrm{m\,s^{-1}}$ which are absent in the INT case. The pdf differences of the cold pool areas between the FIX and INT cases are much more pronounced over LAND than over the OCEAN, with nearly no cold pools larger than $500\,\mathrm{km^2}$ (Figures 4a and 4e) present in the INT case. In the FIX case, 20% of the cold pools are larger than $500\,\mathrm{km^2}$ (Figure 4e). Because of the larger and less numerous cold pools, convection is more organized in the FIX case (not shown).

Similar to the OCEAN scenario, over LAND there are fewer cold pools in FIX (average of 5.6) than in INT (average of 11.15). The larger cold pools present in FIX are associated with smaller gust front velocities (not shown), as discussed for the OCEAN scenario. Unlike the runs over the ocean, however, the distribution of gust front velocities in the INT case is concentrated around smaller values than in the FIX case (Figures 4b and 4f). We attribute this to the large surface buoyancy fluxes—reaching as high as $400\,\mathrm{W\,m^{-2}}$ in the LAND INT case and only $180\,\mathrm{W\,m^{-2}}$ in the OCEAN INT—which rapidly diminish the cold pools' density anomalies. Notice that this rapid recovery is also facilitated by the smaller size cold pools in the INT cases (Figures 4a and 4e). In other words, over LAND the cold pool warming and humidification by spreading and mixing with environmental air in FIX are much smaller than the warming and humidification by surface flux heterogeneity underneath cold pools in INT, whereas they were comparable over the OCEAN.

### 3.2. Changes in Entrainment

As cold pools organize the subcloud layer, they can modify the updraft sizes, their entrainment rate [*Tompkins*, 2001; *Khairoutdinov and Randall*, 2006; *Kuang and Bretherton*, 2006; *D'Andrea et al*., 2014; *Schlemmer and Hohenegger*, 2014] and the number of updrafts. Thus, changes in the cold pool characteristics could translate into modifications of the updraft mass flux and entrainment rates. To understand the reason behind the mass flux changes, we tagged the individual updrafts using the same identification algorithm we used for the cold pools (section 2.3) and computed the average area and MSE of updrafts at the LCL on the model snapshot every half hour for the last 6 h of the simulations.

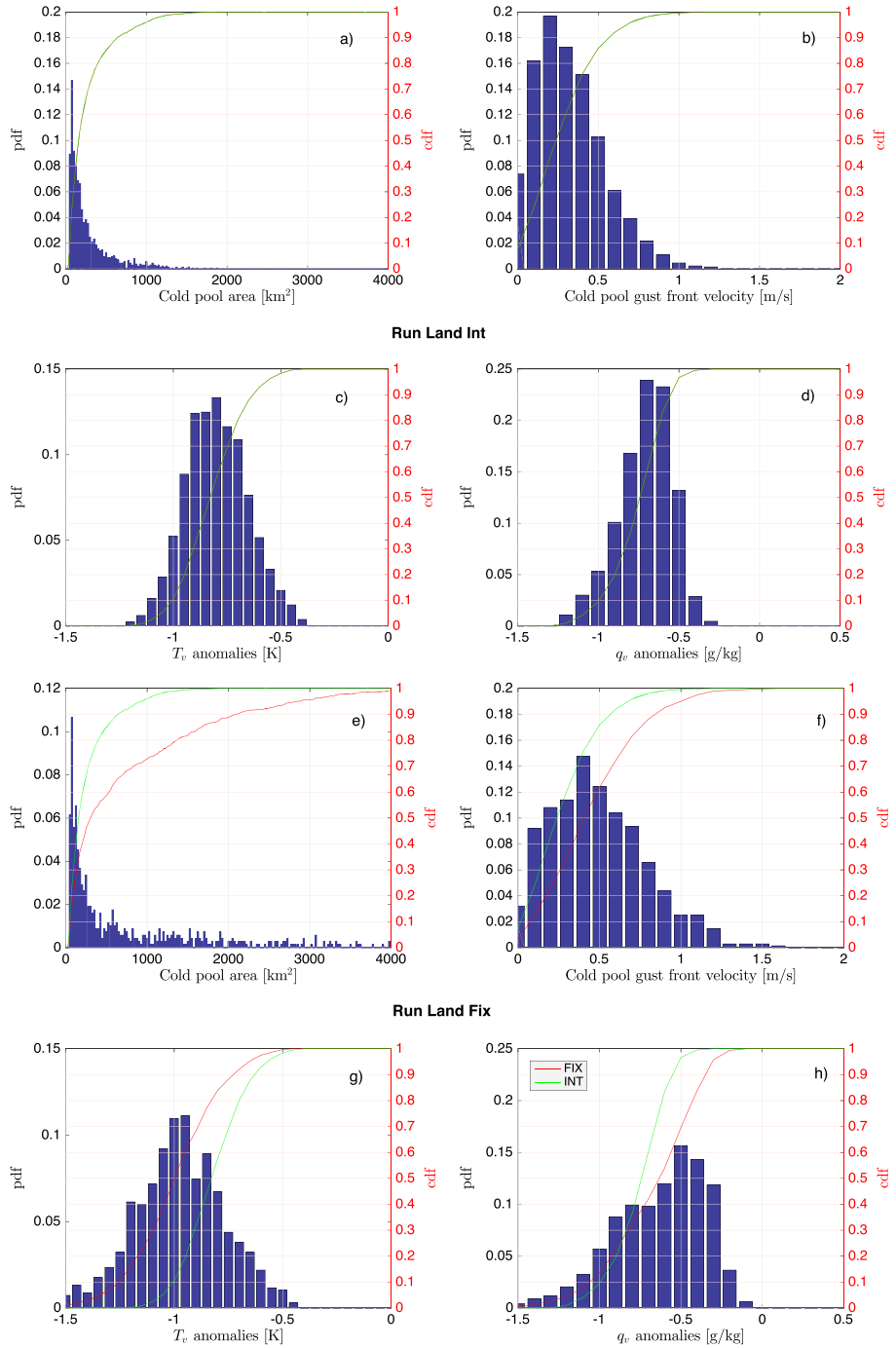


**Figure 4.** Same as Figure 2 but for the LAND case.

Overall, the LAND updrafts have higher MSE than their oceanic counterparts (Figure 5), mostly because of the higher surface heat fluxes (Table S4) [*Gentine et al.*, 2013a, 2013b]. This is evidenced by the typically larger updraft MSE values over LAND (Figure 5). We note that there are only minor changes in the environmental MSE between the two scenarios. The corresponding updraft mass flux is more intense over LAND for any entrainment rate (Figure 2). One of the reasons for this higher mass flux is that the boundary layer is deeper over LAND so that the kinetic energy of the updrafts at cloud base is higher than over the OCEAN, since updrafts accelerate more in a deeper boundary layer [*Gentine et al.*, 2013a, 2013b].

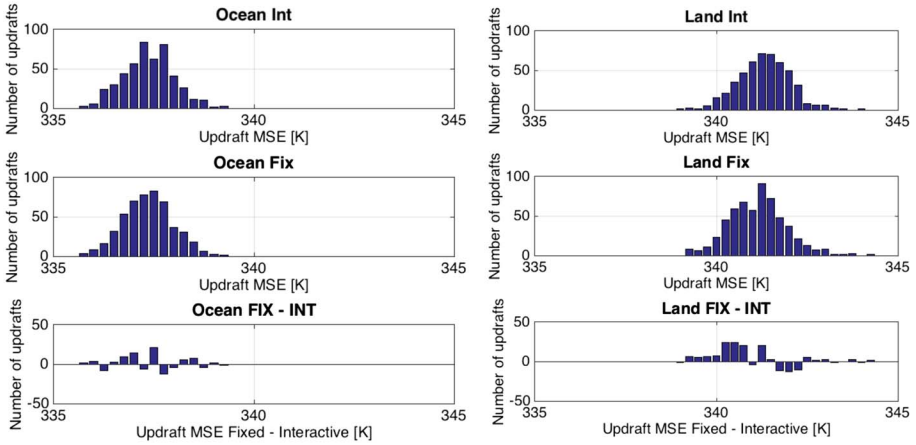


**Figure 5.** Time-averaged (every 30 min for 6 h) distribution of individual updraft MSE at the LCL for the (top) interactive INT and (middle) fixed FIX cases (middle) and their (bottom) differences FIX − INT for the (left column) OCEAN and (right column) LAND cases.

Over the OCEAN, the mass flux is larger in FIX for most entrainment rates (Figure 2, bottom), except for the taller clouds (>6 km) and lowest entrainment rates (<0.3 $km^{-1}$). The mass flux increase is due to the increased number of small area (Figure S2) and low-MSE updrafts (Figure 5). Over LAND, the mass flux is more intense in FIX for the higher entrainment rates $\epsilon > 0.8\,km^{-1}$, corresponding to shallower convection. Those changes are due to the increase in the number of small (Figure S2) and low-MSE updrafts (Figure 5) in FIX. On the other hand, the mass flux is reduced in FIX for the lower entrainment rates $\epsilon < 0.8\,km^{-1}$, corresponding to higher reaching updrafts. This is to be attributed to the increased MSE of the most energetic updrafts in FIX (Figure 5). We suspect that this is due to the increased organization of convection in FIX, which generates more intense thermodynamic anomalies of updrafts [*Schlemmer and Hohenegger*, 2015; *Torri et al*., 2015].

The number of updrafts increases in FIX, especially over LAND, (Figures 5 and S2) as the triggering of new updrafts is increased by wider cold pools. Homogenization of the surface fluxes in the FIX case increases the number of small updrafts (Figure S2) because of the increased intensity of the gust front in FIX, which produces a stronger mechanical lifting of air at the edge of the cold pool [*Jeevanjee and Romps*, 2015; *Torri et al*., 2015] and generates updrafts with higher kinetic energy [*Grandpeix and Lafore*, 2010]. No noticeable difference is seen for the large updrafts (>10 $km^2$) in FIX over the OCEAN, but a slight increase in the number of large updrafts is observable over LAND (Figure S2). The number of low-MSE updrafts increases in FIX over both the OCEAN and LAND (Figure 5). Over LAND, the high-MSE updrafts are more numerous in INT (Figure 5). This increase in higher-MSE updrafts is most likely due to the higher MSE of environmental air in INT, induced by the higher surface fluxes around the cold pools. This air, in turn, directly feeds the updrafts, especially the shallow ones (Figure S2).

## 4. Conclusions

We have investigated the role of surface heat fluxes underneath cold pools using cloud-resolving simulations over an ocean and an idealized land surface, with either interactive or prescribed homogenous surface heat fluxes. We have shown that, over the ocean, there are limited changes in the pdfs of temperature, humidity, and gust front velocity of the cold pools. Nonetheless, the surface heat fluxes underneath cold pools drastically limit the number of large cold pools (>500 $km^2$) and induce more, smaller cold pools, reducing convective organization. As a result, the updraft mass flux, MSE, and lateral entrainment are impacted.

Over land, the heat fluxes underneath cold pools generate more numerous and smaller cold pools, which are warmer and more humid, and have smaller gust front velocities. The updraft mass flux and the lateral entrainment are also substantially affected. The interactive fluxes underneath cold pools reduce the updraft mass flux. In addition, convective organization is reduced in the interactive flux case.

These results emphasize the important role of interactive surface fluxes underneath cold pools when studying deep convection. Deep convection over land surfaces is drastically affected by surface heterogeneity underneath cold pools, which highlights the complication of studying convection over land surfaces. We performed a sensitivity analysis to the Monin-Obukhov stability function by changing the sensitivity to the Obukhov length in the stability functions, which regulate the heat flux response to surface instability. These changes in the stability functions also drastically altered the cold pool and convection characteristics, especially over the land surface. An important conclusion is thus that surface roughness and the parameterization of surface heat flux and stability functions can have a nontrivial impact on deep convection characteristics through modification of the cold pool characteristics. In shallow convection, interactive surface fluxes should be less important since surface fluxes are more homogenous in the horizontal as they are typically not interacting with cold pools. Shear and the diurnal cycle over land could modify some of the conclusions presented here as they will affect convective organization and the size, life cycle, and propagation of cold pools. Shear, in particular, is nontrivial as its position and strength modify the cold pool characteristics. This would substantially complicate the analysis of cold pools so that new tools would need to be introduced to investigate their characteristics.

**Acknowledgments**

P.G and Z.K. would like to acknowledge collaborative DOE funding DE-SC0008720 probing the transition between shallow and deep convection. P.G. acknowledges funding DOE DE-SC0011094 (GoAmazon), DOE early career award DE-SC0014203, and NASA New Investigator Program (NIP) NNX14AI36G: "a unified parameterization of dry and moist convection." The data are accessible on request directed to Pierre Gentine by email.

## References

Betts, A. K. (1974), Scientific basis and objectives of US convection subprogram for GATE, *Bull. Am. Meteorol. Soc.*, *55*(4), 304–313.

Betts, A. K. (1984), Boundary layer thermodynamics of a high plains severe storm, *Mon. Weather Rev.*, *112*(11), 2199–2211, doi:10.1175/1520-0493(1984)112<2199:BLTOAH>2.0.CO;2.

Betts, A. K., and M. F. Silva Dias (1979), Unsaturated downdraft thermodynamics in cumulonimbus, *J. Atmos. Sci.*, *36*, 1061–1071, doi:10.1175/1520-0469(1979)036<1061:UDTIC>2.0.CO;2.

Böing, S. J., H. J. J. Jonker, A. P. Siebesma, and W. W. Grabowski (2012), Influence of the subcloud layer on the development of a deep convective ensemble, *J. Atmos. Sci.*, *69*(9), 2682–2698, doi:10.1175/JAS-D-11-0317.1.

Businger, J., J. Wyngaard, Y. Izumi, and E. Bradley (1971), Flux-profile relationships in the atmospheric surface layer, *J. Atmos. Sci.*, *28*(2), 181–189.

Cronin, T. W., and K. A. Emanuel (2013), The climate time scale in the approach to radiative-convective equilibrium, *J. Adv. Model. Earth Syst.*, *5*, 843–849, doi:10.1002/jame.20049.

D'Andrea, F., P. Gentine, A. K. Betts, and B. R. Lintner (2014), Triggering deep convection with a probabilistic plume model, *J. Atmos. Sci.*, *71*, 3881–3901, doi:10.1175/JAS-D-13-0340.1.

Emanuel, K. A. (1994), *Atmospheric Convection*, Oxford Univ. Press, New York.

Feng, Z., S. Hagos, A. K. Rowe, C. D. Burleyson, M. N. Martini, and S. P. Szoeke (2015), Mechanisms of convective cloud organization by cold pools over tropical warm ocean during the AMIE/DYNAMO field campaign, *J. Adv. Model. Earth Syst.*, *7*, 357–381, doi:10.1002/2014MS000384.

Gentine, P., A. K. Betts, B. R. Lintner, K. L. Findell, C. C. van Heerwaarden, A. Tzella, and F. D'Andrea (2013a), A probabilistic bulk model of coupled mixed layer and convection. Part I: Clear-sky case, *J. Atmos. Sci.*, *70*(6), 1543–1556, doi:10.1175/JAS-D-12-0145.1.

Gentine, P., A. K. Betts, B. R. Lintner, K. L. Findell, C. C. van Heerwaarden, and F. D'Andrea (2013b), A probabilistic bulk model of coupled mixed layer and convection. Part II: Shallow convection case, *J. Atmos. Sci.*, *70*(6), 1557–1576, doi:10.1175/JAS-D-12-0146.1.

Grandpeix, J.-Y., and J.-P. Lafore (2010), A density current parameterization coupled with Emanuel's convection scheme. Part I: The models, *J. Atmos. Sci.*, *67*(4), 881–897, doi:10.1175/2009JAS3044.1.

Jeevanjee, N., and D. M. Romps (2013), Convective self-aggregation, cold pools, and domain size, *Geophys. Res. Lett.*, *40*, 994–998, doi:10.1002/grl.50204.

Jeevanjee, N., and D. M. Romps (2015), Effective buoyancy, inertial pressure, and the mechanical generation of boundary-layer mass flux by cold pools, *J. Atmos. Sci.*, *72*, 3199–3213, doi:10.1175/JAS-D-14-0349.1.

Khairoutdinov, M., and D. Randall (2006), High-resolution simulation of shallow-to-deep convection transition over land, *J. Atmos. Sci.*, *63*(12), 3421–3436.

Khairoutdinov, M. F., and D. A. Randall (2003), Cloud resolving modeling of the ARM summer 1997 IOP: Model formulation, results, uncertainties, and sensitivities, *J. Atmos. Sci.*, *60*(4), 607–625.

Kuang, Z., and C. S. Bretherton (2006), A mass-flux scheme view of a high-resolution simulation of a transition from shallow to deep cumulus convection, *J. Atmos. Sci.*, *63*(7), 1895–1909.

Lafore, J. P., and M. W. Moncrieff (1989), A numerical investigation of the organization and interaction of the convective and stratiform regions of tropical squall lines, *J. Atmos. Sci.*, *46*(4), 521–544, doi:10.1175/1520-0469(1989)046<0521:ANIOTO>2.0.CO;2.

Li, Z., P. Zuidema, and P. Zhu (2014), Simulated convective invigoration processes at trade-wind cumulus cold pool boundaries, *J. Atmos. Sci.*, *71*, 2823–2841, doi:10.1175/JAS-D-13-0184.1.

Liu, C., and M. W. Moncrieff (2004), Effects of convectively generated gravity waves and rotation on the organization of convection, *J. Atmos. Sci.*, *61*(17), 2218–2227, doi:10.1175/1520-0469(2004)061.

Lohou, F., and E. G. Patton (2014), Surface energy balance and buoyancy response to shallow cumulus shading, *J. Atmos. Sci.*, *71*(2), 665–682, doi:10.1175/JAS-D-13-0145.1.

Moncrieff, M. W., and C. Liu (1999), Convection initiation by density currents: Role of convergence, shear, and dynamical organization, *Mon. Weather Rev.*, *127*, 2455–2464.

Morrison, H., and A. Gettelman (2008), A new two-moment bulk stratiform cloud microphysics scheme in the community atmosphere model, version 3 (CAM3). Part I: Description and numerical tests, *J. Clim.*, *21*(15), 3642–3659, doi:10.1175/2008JCLI2105.1.

Muller, C., and S. Bony (2015), What favors convective aggregation and why?, *Geophys. Res. Lett.*, *42*, 5626–5634, doi:10.1002/2015GL064260.

Qian, L., G. S. Young, and W. M. Frank (1998), A convective wake parameterization scheme for use in general circulation models, *Mon. Weather Rev.*, *126*, 456–469.

Ross, A. N., A. M. Tompkins, and D. J. Parker (2004), Simple models of the role of surface fluxes in convective cold pool evolution, *J. Atmos. Sci.*, *61*(13), 1582–1595, doi:10.1175/1520-0469(2004)061.

Schlemmer, L., and C. Hohenegger (2014), The formation of wider and deeper clouds as a result of cold-pool dynamics, *J. Atmos. Sci.*, *71*, 2842–2858, doi:10.1175/JAS-D-13-0170.1.

Schlemmer, L., and C. Hohenegger (2015), Modifications of the atmospheric moisture field as a result of cold-pool dynamics, *Q. J. R. Meteorol. Soc.*, doi:10.1002/qj.2625.

Simpson, J. E. (1969), A comparison between laboratory and atmospheric density currents, *Q. J. R. Meteorol. Soc.*, *95*, 758–765.

Skiena, S. (2008), *The Algorithm Design Manual*, Springer, Berlin, doi:10.1007/978-1-84800-070-4_4.

Tompkins, A. M. (2001), Organization of tropical convection in low vertical wind shears: The role of cold pools, *J. Atmos. Sci.*, *58*(13), 1650–1672, doi:10.1175/1520-0469(2001)058.

Torri, G., Z. Kuang, and Y. Tian (2015), Mechanisms for convection triggering by cold pools, *Geophys. Res. Lett.*, *42*, 1943–1950, doi:10.1002/2015GL063227.

Weisman, M. L., and R. Rotunno (2004), A theory for strong long-lived squall lines revisited, *J. Atmos. Sci.*, *61*(4), 361–382.

Xu, Q., and M. W. Moncrieff (1994), Density current circulations in shear flows, *J. Atmos. Sci.*, *51*(3), 434–446, doi:10.1175/1520-0469(1994)051.